Title
Cellular remodeling of fibrotic conduit as vascular graft

Authors
Qiu, Xuefeng
Lee, Benjamin Li-Ping
Wong, Sze Yue
et al.

Publication Date
2021

DOI
10.1016/j.biomaterials.2020.120565

Peer reviewed

HHS Public Access

Author manuscript

Biomaterials. Author manuscript; available in PMC 2022 January 01.

Published in final edited form as:

Biomaterials. 2021 January ; 268: 120565. doi:10.1016/j.biomaterials.2020.120565.

Cellular Remodeling of Fibrotic Conduit as Vascular Graft

Xuefeng Qiu, M.D.[1,2,3], **Benjamin Li-Ping Lee, Ph.D.**[2], **Sze Yue Wong, Ph.D.**[2], **Xili Ding, Ph.D.**[1], **Kang Xu, Ph.D.**[1,2], **Wen Zhao, Ph.D.**[2,4], **Dong Wang, Ph.D.**[1,2], **Ryan Sochol, Ph.D.**[5], **Nianguo Dong, M.D.**[3,*], **Song Li, Ph.D.**[1,2,6,*]

[1]Department of Bioengineering, University of California, Los Angeles, Los Angeles, CA 90095, USA

[2]Department of Bioengineering, University of California, Berkeley, CA 94720, USA

[3]Department of Cardiovascular Surgery, Union Hospital, Tongji Medical College, Huazhong University of Science and Technology, Wuhan 430022, China

[4]Key Laboratory for Space Biosciences and Biotechnology, School of Life Sciences, Northwestern Polytechnical University, Xi'an, Shanxi 710072, China

[5]Department of Mechanical Engineering, University of Maryland, College Park, MD 20742, USA

[6]Department of Medicine, University of California, Los Angeles, Los Angeles, CA 90095, USA

Abstract

The replacement of small-diameter arteries remains an unmet clinical need. Here we investigated the cellular remodeling of fibrotic conduits as vascular grafts. The formation of fibrotic conduit around subcutaneously implanted mandrels involved not only fibroblasts but also the trans-differentiation of inflammatory cells such as macrophages into fibroblastic cells, as shown by genetic lineage tracing. When fibrotic conduits were implanted as vascular grafts, the patency was low, and many fibrotic cells were found in neointima. Decellularization and anti-thrombogenic coating of fibrotic conduits produced highly patent autografts that remodeled into neoarteries, offering an effective approach to obtain autografts for clinical therapy. While autografts recruited mostly anti-inflammatory macrophages for constructive remodeling, allogenic DFCs had more T

[*]Corresponding to: Song Li, Ph.D. songli@ucla.edu; 5121 Engineering V, The University of California-Los Angeles, Los Angeles, CA 90095; Nianguo Dong, M.D. 1986xh0694@hust.edu.cn; Department of Cardiovascular Surgery, Union Hospital, Tongji Medical College, Huazhong University of Science and Technology, Wuhan 430022, China.

Credit Author Statement

Design experiments: X.Q., B.L.L, S.Y.W., X.D., N.D., S.L.

Perform experiments: X.Q., B.L.L, S.Y.W., X.D., K.X., W.Z., D.W., R.S.

Analyze data: All

Write manuscript: X.Q., B.L.L, S.Y.W., X.D., N.D., S.L

Revise manuscript: X.Q., X.D., N.D., S.L.

Disclosure

None

Declaration of interests

The authors declare that they have no known competing financial interests or personal relationships that could have appeared to influence the work reported in this paper.

cells and pro-inflammatory macrophages and much lower patency. Endothelial progenitors and endothelial migration were observed during endothelialization. Cell infiltration into DFCs was more efficient than decellularized arteries, and infiltrated cells remodeled the matrix and differentiated into smooth muscle cells (SMCs). This work provides insight into the remodeling of fibrotic conduits, autologous DFCs and allogenic DFCs, and will have broad impact on using fibrotic matrix for regenerative engineering.

Keywords

fibrosis; vascular graft; decellularization; inflammatory cells

Subject codes

Translational studies; cardiovascular surgery

Introduction

Vascular grafts are used as replacements for occluded arteries, especially those with multiple and severe lesions, yet small-diameter vascular grafts have low success rate due to frequent thrombus formation and clogging (1). To date, autologous artery and vein remain the gold standard for the replacement of diseased blood vessels. However, many patients do not have appropriate autologous grafts, and vein grafts have a 30~40% failure rate within 5 years (2). Synthetic grafts, such as those made of ePTFE only had ~35% 6-month primary patency rate even with anti-thrombogenic treatment (3). Nano- or micro-fibrous grafts made from non-degradable or biodegradable synthetic polymers have shown some promising results with antithrombogenic treatment or cell seeding to improve biocompatibility (4-12), but the long-term effect of polymer degradation and the graft integration into the host tissue remained to be addressed. On the other hand, scaffolds derived from native extracellular matrix (ECM) have superior cellular compatibility and can be remodeled biologically (13-16). Recent studies on allogenic decellularized vascular grafts made in bioreactor showed promising results in arteriovenous access model (17,18), yet the primary patency of decellularized allogenic grafts needs further improvement (19). Although autologous fibrotic conduits have been explored as vascular grafts, the fibroblastic cells in autografts and the lack of anti-thrombogenic modification are potential drawback for the autograft performance. In addition, the cellular mechanisms of fibrotic conduit formation and graft remodeling need further investigation to improve graft performance.

Here we developed and characterized fibrotic conduits as a source of vascular grafts, and showed that autografts with decellularization and anti-thrombogenic modification had excellent patency rate and could be rapidly remodeled into neoarteries. Autologous decellularized fibrotic conduits (DFCs) is promising for patients who do not have appropriate autologous vascular grafts. Furthermore, we elucidated the mechanisms of cellular remodeling in fibrotic conduits and autografts/allografts, and demonstrated a critical role of immune cells in these processes.

Materials and Methods

Preparation of decellularized vascular grafts

To prepare decellularized vascular grafts, Teflon mandrels were implanted into the subcutaneous pouches in the abdominal wall of Sprague-Dawley rats for 2, 3, 4, and 5 weeks respectively. At each time point, the implants were removed and the outer layer tubular connective tissues were detached from the Teflon mandrels. These fibrotic conduits were decellularized in a series of detergents. Briefly, samples were washed thoroughly in 1M NaCl, then treated with the zwitterionic 3-[(3-Cholamidopropyl) dimethylammonio]-1-propanesulfonate-(CHAPS, Sigma) detergent solution (8mM CHAPS, 1M NaCl, 25mM EDTA) for three times of 2 hours each. Decellularized native arteries underwent a further decellularization in an ionic SDS (Fisher Scientific) detergent (1.8mM Sodium dodecyl sulfate, 1M NaCl, 25mM EDTA). Both DFCs and native arteries were then subjected to a 16 hours benzoase nuclease (Sigma) treatment (90U/ml, 50mM Tris-Cl) before being chemically conjugated with heparin. All samples were rinsed thrice with PBS and stored at 4°C for further use. All treatments were performed at room temperature.

Protein and DNA analysis of decellularized grafts

Each decellularized sample (2-cm long) was homogenized in C-tubes (Miltenyl Biotec) on the gentle MACs dissociator (Miltenyl Biotec) with 300 uL of lysis buffer (G-biosciences) supplemented with protease inhibitors (PMSF, Na_3VO_4 and leupeptin). After centrifugation, the supernatant was collected then quantified using the DC protein assay (Bio-Rad). Samples (10 ug/well) were separated by SDS-PAGE (10% gel) and transferred onto PVDF membranes. The membranes were blocked in 3% non-fat milk and incubated at 4°C overnight with primary antibodies against fibronectin (ab2413; Abcam, 1:2000), actin (sc-1616; Santa Cruz, 1:1000), α-SMA (ab32575; Abcam, 1:5000), calponin-1 (ab46794; Abcam, 1:10000), FSP1 (ab27957; Abcam, 1:1000), and GAPDH (ab8245; Abcam, 1:2000). Membranes were incubated with HRP-conjugated IgG secondary antibodies (Santa Cruz Biotechnologies, 1:2000), and protein bands were visualized using Western Lightning Plus-Enhanced Chemiluminescence Substrate (Perkin Elmer Life & Analytical Sciences) on a digital imager (Bio-Rad).

To measure DNA content, the tissue samples with or without decellularization were digested in papain solution under high temperature (60°C for 24) and low pH conditions (for 24 hours). A DNeasy Blood & Tissue Kit® (Qiagen, Valencia, CA) was used to isolate DNA. The DNA content was quantified by using a Quant-iT™ PicoGreen® Assay (Invitrogen, Grand Island, NY), allowing the detection of DNA at an emission wavelength of 535 nm. The DNA content is normalized by the dry weight of respective tissue samples.

Rat studies

Animal protocols approved by the Committee on Animal Care and Use at the University of California, Berkeley and the University of California, Los Angeles following NIH guidelines for the care and use of laboratory animals. Female Sprague-Dawley rats (body weight: 500-550g, Charles River Laboratories, Boston, MA) were used for experiments. For the comparison of autografts and allografts, each rat was implanted with two Teflon mandrels to

prepare DFCs, one being used as autografts and another one as allografts. Decellularized native common carotid arteries were used for control group. Interpositional implantations were performed in rat common carotid arteries. Briefly, a left neck incision exposed the common carotid artery in rats anesthetized by isoflurane inhalation. The left common carotid artery was cross-clamped, a 4-mm segment was transected and the graft (10 mm in length) was inserted in the gap. End-to-end anastomosis with 9-0 nylon suture (AROSurgical, Newport beach, CA) was used to connect grafts to the native artery. The artery lumen was washed once with heparin solution during the period of surgery. Rats received no other postoperative anticoagulation treatment. Doppler ultrasound was used to detect blood flow and patency in grafts before explantation at various time points.

Lineage tracing of inflammatory cells in mouse model

Vav1-cre, FSP1-cre and ROSA26-enhanced yellow fluorescent protein (R26R-EYFP) mice were purchased from the Jackson Laboratory. Male Vav1-cre mice were crossed with female R26R-EYFP mice to generate Vav1-EYFP mice in which $Vav1^+$ cells (mainly hematopoietic cells/macrophages) were labeled in EYFP to determine their fate such as trans-differentiation into fibroblasts. Similarly, FSP1-EYFP mice were generated by breeding FSP1-Cre and R26R-EYFP mice to label $FSP1^+$ fibroblasts. Genotyping was performed by polymerase chain reaction according to the protocols provided by the Jackson Laboratory. The transgenic mice of two months were used for experiments. Both male and female mice were used, and no sex difference in lineage tracing was detected. Teflon mandrels were implanted subcutaneously. After 1 week or 4 weeks, the Teflon mandrels were harvested for the histological analysis of the fibrotic conduits around the mandrels.

Histological Analysis

Samples for histological examination were snap-frozen in optimal cutting temperature (OCT) Compound (Tissue Tek), and sectioned to 8-μm thickness. Immunofluorescence staining was used to analyze the tissue sections with the following primary antibodies: FSP-1, α-SMA, CD68, CCR7, CD163, CD206, CD3, CD4, FoxP3, CD19, CD31, CD34, von Willebrand factor (vWF), Type I Collagen, Elastin, CNN1, SM-MHC. The information of antibodies is summarized in Supplementary Table 1. Primary antibodies were incubated overnight at 4°C followed by 1hr incubation with Alexa Fluor® 488- and/or Alexa Fluor® 546-conjugated secondary antibodies raised in donkey (Molecular Probes). Nuclei were stained with 4', 6-diamino-2-phenylindole (DAPI; Invitrogen). As negative controls, no-specific mouse or rabbit IgGs were used for staining procedure, showing no signals as expected (Supplementary Fig. 1). Hematoxylin and eosin (H&E), Masson’s trichrome and Verhoeff’s stainings were performed using the kits from American MasterTech Scientific. Inc according to the manufacturer's instruction. Immunofluorescence images were captured with a Zeiss confocal microscope (LSM710), bright-field images were recorded by light microscope (Zeiss). Immunofluorescence images of the whole longitudinal graft were captured with Nano Zommer (Fluorescence Unit L11600/L10387-0, Hamamatsu Photonics K.K., Japan).

En face immunofluorescence staining

The grafts were explanted and fixed with 4% paraformaldehyde for 30 minutes. Each graft was cut into 4 slices longitudinally with “no-touch” technology. The samples were washed with PBS, blocked with 1% donkey serum albumin solution, and incubated with primary antibodies for CD34, CD31, and vWF. After that, samples were incubated with Alexa-Fluor 488 or Alexa-Fluor 546 labeled secondary antibodies raised in donkey (Molecular Probes) and nuclei stained with 4',6-diamino-2-phenylindole (DAPI; Invitrogen). Images were collected on a confocal microscope.

Mechanical Testing

Fresh graft segments of 1 mm in diameter and 1.5-2 mm in width were prepared and subjected to uniaxial tensile testing in the radial direction using an Instron 5544 tester (Instron, Canton, MA) as described previously. Briefly, two 0.3mm-diameter stainless steel wires were placed through the lumen of the ring segment of the graft and loaded in between the grips. Each segment was extended at a rate of 0.1 mm/sec until failure and the applied force and deformation was recorded via Bluehill software (Instron). The elastic modulus was calculated based on the applied load, deformation, and dimensions (thickness and width) of the graft segments; the ultimate tensile strength was recorded as the peak stress prior to failure. Suture tension of DFCs, native common carotid arteries, and 9-0 suture were also tested. Burst pressure was measured as previously described (MFCS™-EZ microfluidic flow control system, Fluigent, Germany).

Electron microscopy imaging

For scan electron microscopy (SEM), the vascular grafts were fixed, dehydrated and dried according to the previous protocol. All specimens were mounted on aluminium stubs using sticky carbon taps and coated with a thin layer of Au/Pd (approximately 2 nm thick) using a Gatan ion beam coater. Images were recorded with a Hitachi TM-1000 scanning electron microscope. For transmission electron microscopy (TEM), all fixed samples were pretreated and sliced according to TEM standard protocol. The stained ultrathin sections were examined on a FEI Tecnai transmission electron microscope and recorded via a SIS Mega View III high resolution CCD camera.

Collagen and Elastin quantification

Collagen and elastin content of the grafts were measured and quantified using respectively the Sircol™ soluble collagen assay and Fastin™ Elastin Assay Kit (both from Biocolor, UK) under manufacturer's instruction.

Mini-pig studies

Female mini-pigs (weighing 25-30 kg) were used a large animal model. Teflon mandrels (4 mm in diameter) were implanted subcutaneously for 4 weeks to generate fibrotic conduits, decellularized, conjugated with heparin, and used as autologous or allogenic DFCs. The DFCs were implanted as interpositional vascular grafts in carotid arteries. After 1-month implantation, the patency of the grafts was examined by computed topography angiography.

Statistical Analysis

All the data were analyzed using Graphpad Prism 7.0 and expressed as mean ± one standard deviation (SD). Student's t-test was used for two-sample statistical comparison, while one-way analysis of variance (ANOVA) followed by Tukey's test was used for groups greater than two A value of $p < 0.05$ was accepted as statistically significant.

Results

Involvement of fibroblasts and macrophages in the formation of fibrotic capsule tissues

To generate fibrotic conduits, we implanted Teflon mandrels subcutaneously into rats. The robust fibrotic tissue formation resulted in a tubular structure with sufficient mechanical strength within 2-4 weeks. Various cells contributed to fibrotic capsule formation. Fibroblasts (fibroblast-specific protein 1-positive/ $FSP1^+$) and myofibroblasts (smooth muscle α-actin-positive/α-SMA^+) were found in the tissue capsule during the 4-week remodeling period (Fig. 1a).

Immune responses were found to play an important role in fibrotic capsule formation (20). Macrophages, T cells and B cells were recruited as early as day 3 but showed different temporal kinetics (Fig. 1b-e). To determine the phenotype of macrophages, the samples were stained for CD68 (pan-macrophage cell surface marker), CCR7 (pro-inflmmatory macrophage marker) or CD163 (anti-inflammatory marker). $CCR7^+$ macrophages reached highest level at day 3, mostly found at the interface of the capsule tissue and the mandrel, indicating a foreign-body response at the early stage, and then gradually disappeared after day 7. In contrast, the number of $CD163^+$ anti-inflammatory macrophages reached the peak around day 7, indicating the initiation of constructive remodeling of the capsule tissue. Staining for CD206, another anti-inflammatory macrophage marker, showed colocalization with CD163 (Supplementary Fig. 1), so we used either CD163 or CD206 to identify anti-inflammatory macrophages in the following studies. $CD3^+$ T cells, $CD4^+$ T helper cells or $FoxP3^+$ regulatory T cells also showed a peak level at day 7. Few B cells were found in capsule tissues.

Interestingly, after 7 days, we observed that some $CD206^+$ or $CCR7^+$ macrophages expressed FSP1, a fibroblast marker (Supplementary Fig. 2). To directly test whether macrophages could trans-differentiate into fibroblastic cells, we performed lineage tracing experiments by implanting Teflon mandrels subcutaneously in Vav1- EYFP mice in which the cells derived from $Vav1^+$ hematopoietic cells were labeled by EYFP. As shown in Figure 2, most $EYFP^+$ cells in fibrotic tissue were positive for CD45 (hematopoietic marker), CD68 (pan-macrophage marker), CCR7 and CD206, suggesting that macrophages were a major population of $EYFP^+$ cells. Interestingly, after 7 days, many $EYFP^+$ cells expressed FSP1 (Fig. 2), a fibroblast marker, but not CD31, an endothelial cell (EC) marker; and a small percentage of cells next to the surface of the mandrel expressed α-SMA, a myofibroblast marker (Fig. 2), implying that inflammatory cells could trans-differentiate into fibroblast-like cells and participate in the remodeling of fibrotic capsule tissues. Furthermore, at 4 weeks, most Vav1-EYFP cells became FSP1+ and SMA+ (Supplementary Fig. 3). Consistently, when we implanted Teflon mandrels subcutaneously in FSP1-EYFP mice, we

found that macrophages ($CD68^+$) became $EYFP^+$ at day 7, suggesting a trans-differentiation into fibroblast-like cells (Supplementary Fig. 4).

Cells in fibrotic conduits were involved in neointima formation

After 4 weeks, fibrotic conduits were harvested as vascular grafts. Fibrotic conduits with cells were previously used as arteriovenous graft with acceptable patency due to high flow rate and a drastic pressure drop from artery to vein; however, for other artery replacement, significant thrombosis and neointima formation were observed for autologous grafts containing fibrotic cells (21,22). In our study, we found that the patency rates of fibrotic conduits were 4 out of 9 after 2 weeks and 1 out of 9 after two months. An example of fibrotic conduit before and right after implantation is shown in Supplementary Figure 5a-b. In some cases, the grafts were clogged at early stage by day 14, possibly due to thrombus formation (Supplementary Fig. 5c). In patent grafts, some SMCs can be observed after 4 weeks (Supplementary Fig. 5d). To determine whether the fibrotic cells were involved in neointima formation, we made fibrotic conduits by implanting the cylindrical Teflon mandrel subcutaneously into transgenic Sprague-Dawley rats (n=6) expressing green fluorescence protein (GFP) (Fig. 3a). The gross appearance of a fibrotic conduit right after explantation is shown in Fig. 3b. These grafts with GFP^+ cells were then implanted into wild-type Sprague-Dawley rats with the immunosuppression using Cyclosporin A (CyA, 6 mg/kg, Novartis Pharma AG, Switzerland). The graft was explanted 4 weeks later, showing neointima formation (Fig. 3c), and ~86% of neointimal cells were GFP^+ (Fig. 3d). Although it remained to be determined whether and how these fibrotic cells contributed to immunogenic responses, proliferative cell population and/or matrix deposition, our findings suggested that removing fibrotic cells could improve patency, which also offered an additional benefit of making the grafts available-off-the-shelf.

Decellularization of fibrotic conduits

Detergents of various strengths and properties have been used to remove cells and extracellular components from tissues. Ionic detergents such as sodium dodecyl sulfate (SDS) can lyse cells efficiently, but may damage ECM, leave behind residues, and compromise cell-ECM interactions. Since newly formed fibrotic ECM were not as dense as that in native artery, we used milder zwitterionic detergent (3-[(3-cholamidopropyl)dimethylammonio]-1-propanesulfonate (CHAPS) to decellularize the fibrotic tissues. The overall experiment procedure for the preparation, implantation and characterization of DFCs is shown in Fig. 4a. Following the explantation of the fibrotic conduits, we used a CHAPS-based solution to decellularize the grafts, which preserved the ECM structure, as shown in Fig. 4b-f. Histological analysis indicated that decellularization with CHAPs preserved the major structural collagen (Fig. 4c-d). Elastin was not observed in fibrotic tissues, either before or after decellularization (Fig. 4e-f). This decellularization process completely removed cell nuclei (Fig. 4g-h) and major cellular proteins (Fig. 4i) in the fibrotic tissue. Quantitative DNA detection showed that DNA content dropped 0.05 mg/mg (tissue dry weight) after decellularization (Supplementary Fig. 6). High magnification scanning electron microscopy (SEM) of the decellularized grafts showed that DFCs had less dense fibers of ECM on both inner (Fig. 4j) and outer (Fig. 4k) surface, which is advantageous for cell infiltration compared to the densely packed ECM in

decellularized thoracic aorta (Supplementary Fig. 7). Indeed, interpositional transplantation of decellularized thoracic aorta into carotid artery showed neointima in the lumen but little cell infiltration into the dense ECM (Supplementary Fig. 7e), which could compromise the remodeling and integration of the decellularized thoracic aorta.

Mechanical properties of fibrotic conduits

To determine the implantation time and decellularization process on the mechanical properties of fibrotic conduits, we compared the pre- and post-decellularization mechanical properties of grafts that were implanted subcutaneously for 2-5 weeks. We observed a significant increase in the Young's modulus and ultimate tensile strength (UTS) of grafts with time and a plateau after 4 weeks, suggesting that 4-week implantation was sufficient (Fig. 4l, m). In addition, the decellularization process did not significantly alter the Young's modulus and UTS (Fig. 4l, m). Thus, only grafts formed at 4-week time point were used for further studies. The suture retention of the DFC was significantly higher than the break force of a 9-0 suture although it was lower than that of the native artery (Fig. 4n).

Implantation patency and endothelialization of DFCs

Since collagen-based ECM is highly thrombogenic, we conjugated heparin to the surface of the fibrotic conduits to form an anti-thrombogenic coating. As shown in Figure 4o, the grafts in phosphate buffered saline (PBS) under flow condition still retained ~70% of heparin after 7 days, and no difference was observed for DFCs and decellularized arteries.

To assess the *in vivo* performance of DFCs as vascular grafts, we implanted the grafts into rat carotid arteries by anastomosis. First, we examined the long-term graft patency at multiple time points for both autologous and allogenic grafts. Representative gross image of an implanted autologous DFCs is shown in Fig. 5a, and ultrasound imaging was used to determine the patency of the DFCs (Fig. 5b). The cross-section and longitudinal section of patent grafts at 90 days post implantation are exemplified in Fig. 5c and Fig. 5d respectively. We found that autologous DFCs had much higher patency (94.1%, 16 patent grafts/17 total) than allogenic DFCs (52.9%, 9 patent grafts/17 total grafts) at 90 days (Fig. 5e, Movie 1). This overall graft patency was also higher than the previous reported grafts made with similar approach but with no decellularization (23). Similarly, the patency rates for 14 and 28 days were 88% (6/7) and 100% (7/7) for autologous DFCs, respectively, compared to the patency rates of allogenic DFCs at 71% (5/7) and 57% (4/7) (Supplementary Fig. 8). Significant neointima formation was only found in 12% of autografts, as exemplified in Supplementary Figure 9. Furthermore, long-term studies showed excellent patency of autografts at 180 days (100%, n=7). DFCs were mechanically stable upon implantation, and there was no significant increase in the luminal cross-section area of DFCs, suggesting that there was no aneurysmal dilation for up to 180 days post implantation (Fig. 5f, Movie 2).

To investigate whether patent DFCs had rapid endothelialization on the luminal surface of the grafts, *en face* and cross-section staining for ECs was performed (Fig. 5g-k, m-q). Near anastomotic sites, mature ECs could migrate from the adjacent arteries (Fig. 5g, m). ECs formed a monolayer to cover the inner surface of the autografts after day 14 (Fig. 5i-k). Staining of vWF also showed consistent EC lining on the inner lumen of the graft (Fig. 5o-

q). In contrast, allogenic DFCs had incomplete endothelialization at day 14, and EC monolayer still did not fully form in some region at day 28 (Supplementary Fig. 10). In the middle section of the grafts, $CD34^+/CD31^+$ cells were observed at day 7 (Fig. 5t), suggesting that $CD34^+$ endothelial progenitor cells (EPCs) from the blood stream attached to the luminal surface, which differentiated into ECs ($CD31^+$) (day 14, Fig. 5u, v). These results suggest that ECs might migrate from the adjacent native arteries and that $CD34^+$ EPCs could be recruited from the blood stream.

Involvement of inflammatory cells in the remodeling of vascular wall

Inflammatory responses play an important role in vascular graft patency and remodeling. The number $CD68^+$ macrophages was not significantly different between autologous and allogenic DFCs at days 3 and 14, but there were more $CD68^+$ cells in autologous DFCs at day 28 (Fig. 6a, b, c). Macrophage was absent after the completion of remodeling at day 90 (data not shown). Close examination showed that autologous DFCs had more $CD163^+$ macrophages while allogenic DFCs had more $CCR7^+$ macrophages (Fig. 6a, d, e), and the increase of $CD163^+$ macrophages at day 28 accounted for the increase of $CD68^+$ cells, implying the constructive remodeling of autografts. In addition, significantly more T cells ($CD3^+$) were observed in allografts at days 3, 14, 28, indicating a strong adaptive immune response to allogenic grafts (Fig. 6b, f, g). Furthermore, we found a significant increase in $CD4^+$ and $FoxP3^+$ cells in the allogenic DFCs at day 3 (Fig. 6b, g, h), indicating that these T cells might modulate a foreign body response to allografts (24), possibly caused by the allogenic proteins and DNA residue in decellularized matrix.

Remodeling of ECM in DFCs

To evaluate ECM remodeling in autologous DFCs, we stained samples explanted at days14, 28, 90 and 180 post-implantation for collagen and elastin, the major ECM components accounting for the mechanical strength of blood vessel. While only a loose fibrous mesh of collagen and elastin was observed initially at 14 days (Fig. 7a), ECM fibers increased at days 28 and 90 (Fig. 7b, c), and showed a mature organized structure of densely layered collagen and elastin in an interconnecting lamellar network at day 180 (Fig. 7d), similar to that in native arteries (Fig. 7e). We further quantified the contents of collagen and elastin, and found no significant difference between regenerated arteries and native arteries (Fig. 7f); in addition, the elastin/collagen ratio was also similar (Fig. 7g). We then performed mechanical tests on neoarteries remodeled from autologous DFCs at 90 days post implantation, and found similar Young's modulus (Fig. 7h) and UTS (Fig. 7i) between the neoarteries and native arteries. Before implantation (Day 0), DFCs had a significantly lower burst pressure but *in vivo* remodeling eventually resulted in neoarteries capable of withstanding burst pressures similar to native arteries (Fig. 7j). No calcification was observed in autologous DFCs for up to 3 or 6 months post-implantation (Supplementary Fig. 11). Immunostaining and transmission electron microscopy (TEM) analysis at day 90 also showed the presence of a basement membrane below the newly formed endothelium, similar to that in native artery (Supplementary Fig. 12). On the other hand, allografts, if patent, also had similar remodeling of collagen and elastin (Supplementary Fig. 13a-b). However, calcification was present in allografts after 90 days (Supplementary Fig. 13c), which could contribute to the low efficiency of allografts.

Cellular remodeling in the wall of DFCs

Cell infiltration is a major determinant of graft remodeling. Histological evaluation of the autologous grafts explanted at days 14, 28, 90 and 180 showed a time-dependent cell infiltration. At day 14 (Fig. 8a), there was an infiltration of small percentage of SMCs positive for α-SMA, calponin-1 or smooth muscle myosin heavy chain (smMHC). After 28 days, cell numbers continued to increase, with more SMCs (Fig. 8b). Similar to the that during the formation of subcutaneous fibrotic tissues, we found evidence that some macrophages near the lumen of the grafts trans-differentiated into SMCs (Supplementary Fig. 14). On the other hand, allografts, if patent, also showed similar cell infiltration into the wall (Supplementary Fig. 10). Remodeling was largely completed by 90 days post-implantation (Fig. 8c), with layers of SMCs as the major cell type in the wall, and there was an organized layered structure by 180 days post-implantation (Fig. 8d), closely resembling the tunica media in a native artery (Fig. 8e). Most importantly, no obvious neointima was observed in the patent samples. This is in contrast to the decellularized thoracic aorta samples where few cells were observed to have infiltrated into the vessel wall even after 90 days of implantation, although there was a significant neointima formation (Supplementary Fig. 7e).

Further examination of longitudinal sections of the autologous DFCs showed that host cell infiltration and matrix remodeling had occurred throughout the entire length of the graft by 90 days post-implantation (Fig. 8f). The representative image of the full length of the DFC and the magnified images of the anastomoses and mid-graft at day 90 demonstrated the presence of a continuous band of SMCs and a layer of ECs throughout the length of the graft. In addition, pericytes and vasa vasorum were also observed around the outer graft wall. To gain a deeper understanding of the temporal occurrence of cellular events associated with the formation of *vasa vasorum,* we studied samples at 28, 90 days post-implantation, respectively. We observed ECs in the outer graft wall at 28 days (Supplementary Fig. 15a), while the mature vasa vasorum were observed at 90 days with perivascular cells (Supplementary Fig. 15b). We quantified the number of microvessels that had developed around the outer surface of the graft at day 90 and found no significant difference between the autologous DFC-derived neoartery and native arteries (Fig. 8g). The formation of *vasa vasorum* around DFCs might facilitate the remodeling throughout the length of the graft.

In vivo patency of DFCs in mini-pig model

To investigate whether DFCs have similar patency in a large animal model, we implanted autografts or allografts into the carotid arteries of mini-pigs. As shown in Supplementary Figure 16, autografts had a higher patency (9 out of 10) in comparison to allografts (6 out of 10) at 1-month time point, consistent with the trend in the rat model. These results also demonstrated the potential of DFCs for clinical applications.

Discussion

Autologous DFCs demonstrate higher patency than allogenic DFCs, and show more effective remodeling than decellularized arteries, which offers a promising graft source for patients who do not have appropriate autologous vascular grafts and otherwise would need

peripheral arterial therapy or tissue/organ-specific treatment (26,27). For clinical practice, the procedure will involve three-steps for autografts: (1) subcutaneous implantation of a Teflon mandrel to generate customized size of an autologous fibrotic conduit, (2) retrieve the fibrotic conduit for decellularization and anti-thrombogenic modification, and (3) implant the DFC as a vascular graft. The formation of fibrotic conduits *in vivo* is more robust than the matrix synthesis in cell culture, resulting in a tubular structure with sufficient mechanical strength within 4 weeks. Since fibroblasts in fibrotic conduits participate in thrombosis and neointima formation (21, 28-31), fibrotic conduits were decellularized by using a CHAPS-based protocol that removed the cells but retained the ECM structure and mechanical property. These DFCs have newly synthesized ECM that is less dense than native arteries and allow efficient cell infiltration and remodeling.

The investigation on inflammatory cells revealed that macrophages play an important role in the formation of fibrotic conduits and the remodeling of vascular grafts. Interestingly, lineage tracing studies suggest that macrophages may trans-differentiate into fibroblastic cells and contribute to fibrotic tissue formation as early as day 7, and similar mechanism may also contribute to SMC formation during vascular remodeling. This potential cell type conversion is well correlated with the decrease of macrophages after day 7 and the constructive remodeling in fibrotic tissues, consistent with our finding on the role of bone marrow cells in fibrotic tissue formation (47). One major difference in immune responses to autografts and allografts was the higher $CD163^+$ macrophages and lower $CCR7^+$ macrophages in autografts, which could result in different remodeling process; in addition, allografts had higher level of T cell recruitment, all of which may contribute to the significant difference in the patency rate of autografts and allografts. Whether immunomodulation can improve the patency of allogenic DFCs remained to be investigated.

Autologous DFCs enables rapid endothelialization within 2 weeks, in comparison to incomplete endothelialization in allografts (Supplementary Fig. 10). There is evidence that circulating EPCs contribute to the EC regeneration in addition to EC migration from adjacent arteries at the proximal and distal ends (44). Additionally, generation of a basement membrane is important to maintain the underlying SMCs quiescent to prevent intimal hyperplasia (7). The cells recruited to the decellularized grafts appear to be heterogeneous, including inflammatory cells, SMCs and other cell types such as fibroblasts and mesenchymal stem cells (45). For example, we did observe a small percentage of $C\text{-}kit^+$ perivascular cells were recruited to DFCs (data not shown) (25). During regeneration, ECs may form a monolayer to suppress the activation and adhesion of platelets, monocytes and other immune cells, but it is not clear whether EC could be fully functional by forming tight junctions to regulate the permeability of macromolecules. Since cytokines released from immune cells can increase EC permeability, it is likely that EC monolayer in the regenerating grafts is partially permeable.

The infiltrated cells remodel ECM by depositing proteins such as type I collagen and elastin and modifying the structure. At 90 days post-implant, examination of the graft reveals the neoarteries derived from DFCs have mechanical properties similar to normal arteries in Young's modulus, UTS and burst pressure. The elastin to collagen ratio is 0.40±0.05,

compared to 0.41±0.03 of native arteries. Since DFCs start with native ECM, there is advantage over polymer grafts that require polymer degradation during remodeling process.

Previous studies on fibrotic conduits as vascular grafts include both cellular grafts and acellular grafts (14,15,17,20,32-36). Although cellular fibrotic grafts are convenient to use, especially as dialysis grafts that experience a high flow rate due to arteriovenous bypass, the patency is much lower due to potential thrombus and neointima formation (10, 37, 38). By using fibrotic conduits made in GFP transgenic rat model, we provide direct evidence that fibroblasts in the fibrotic conduits are a major cell source in neointima hyperplasia. Some studies remove cells by using detergents or even crosslinking chemicals, which do not show effective cell infiltration (39,40,41). We have developed a protocol that significantly improves the DFC performance. First, our protocol does not require SDS for decellularization, avoiding the need for the harsh detergent which was previously suggested to be associated with graft calcification. Secondly, cell infiltration into our DFCs is highly efficient, indicating an excellent ECM structure and niche for host cell repopulation. Thirdly, our DFCs demonstrate superior post-operative immune response., with a higher percentage of anti-inflammatory macrophages participating in constructive DFC remodeling (24,42). Fourthly, the formation of *vasa vasorum* in the outer layer of the DFCs allows efficient transport of oxygen and nutrients to facilitates graft remodeling by providing necessary nutrients (43).

In summary, the DFCs developed in this study show encouraging results in both rat and mini-pig models. We envision DFCs can be used for the replacement of coronary artery, peripheral arteries and AV shunts (46), which can be expanded to many other applications such as the regeneration of bladder and ureter.

Supplementary Material

Refer to Web version on PubMed Central for supplementary material.

Acknowledgements

We thank the technical assistance of animal core facilities at the University of California-Berkeley and The University of California-Los Angeles.

Sources of Funding

This work was supported in part by the grants from the National Institute of Health (EB012240, HL083900 and HL121450 to S.L.) and California Institute for Regenerative Medicine (a clinical fellow’s training grant TG2-01164 to X.Q.) at UC Berkeley.

Data Availability

The raw/processed data required to reproduce these findings cannot be shared at this time due to technical or time limitations. We will get the data ready before publication.

References

1. Seifu DG, Purnama A, Mequanint K, Mantovani D. Small-diameter vascular tissue engineering. Nat Rev Cardiol, 2013, 10(7):410–21. [PubMed: 23689702]

2. Hess CN, Lopes RD, Gibson CM, Hager R, Wojdyla DM, Englum BR, Mack MJ, Califf RM, Kouchoukos NT, Peterson ED, Alexander JH. Saphenous vein graft failure after coronary artery bypass surgery: insights from PREVENT IV. Circulation, 2014, 130(17): 1445–51. [PubMed: 25261549]

3. Shemesh D, Goldin I, Hijazi J, Zaghal I, Berelowitz D, Verstandig A, Olsha O. A prospective randomized study of heparin-bonded graft (Propaten) versus standard graft in prosthetic arteriovenous access. J Vasc Surg. 2015,62(1): 115–22. [PubMed: 25770987]

4. Yu J, Wang A, Tang Z, Henry J, Li-Ping Lee B, Zhu Y, Yuan F, Huang F, Li S. The effect of stromal cell-derived factor-1alpha/heparin coating of biodegradable vascular grafts on the recruitment of both endothelial and smooth muscle progenitor cells for accelerated regeneration. Biomaterials, 2012, 33(32):8062–8074. [PubMed: 22884813]

5. Qiu X, Lee BL, Ning X, Murthy N, Dong N, Li S. End-point immobilization of heparin on plasma-treated surface of electrospun polycarbonate-urethane vascular graft. Acta Biomater, 2017, 15(51): 138–147.

6. McClure MJ, Simpson DG, Bowlin GL. Tri-layered vascular grafts composed of polycaprolactone, elastin, collagen, and silk: Optimization of graft properties. J Mech Behav Biomed Mater, 2012, 10:48–61. [PubMed: 22520418]

7. Wu W, Allen RA, Wang Y. Fast-degrading elastomer enables rapid remodeling of a cell-free synthetic graft into a neoartery. Nat Med, 2012, 18(7): 1148–53. [PubMed: 22729285]

8. Roh JD, Sawh-Martinez R, Brennan MP, Jay SM, Devine L, Rao DA, Yi T, Mirensky TL, Nalbandian A, Udelsman B, Hibino N, Shinoka T, Saltzman WM, Snyder E, Kyriakides TR, Pober JS, Breuer CK. Tissue-engineered vascular grafts transform into mature blood vessels via an inflammation-mediated process of vascular remodeling. Proc Natl Acad Sci U S A, 2010, 107(10):4669–74. [PubMed: 20207947]

9. Wu P, Wang L, Li W, Zhang Y, Wu Y, Zhi D, Wang H, Wang L, Kong D, Zhu M. Construction of vascular graft with circumferentially oriented microchannels for improving artery regeneration. Biomaterials, 2020, 242:119922. [PubMed: 32155476]

10. Tillman BW, Yazdani SK, Neff LP, Corriere MA, Christ GJ, Soker S, Atala A, Geary RL, Yoo JJ. Bioengineered vascular access maintains structural integrity in response to arteriovenous flow and repeated needle puncture. J Vase Surg, 2012, 56(3):783–793.

11. Haskett DG, Saleh KS, Lorentz KL, Josowitz AD, Luketich SK, Weinbaum JS, Kokai LE, D Amore A, Marra KG, Rubin JP, Wagner WR, Vorp DA. An exploratory study on the preparation and evaluation of a “same-day”‘ adipose stem cell–based tissue-engineered vascular graft. J Thorac Cardiovasc Surg, 2018, 156(5): 1814–1822. [PubMed: 30057192]

12. Hibino N, McGillicuddy E, Matsumura G, Ichihara Y, Naito Y, Breuer C, Shinoka T. Late-term results of tissue-engineered vascular grafts in humans. J Thorac Cardiovasc Surg, 2010, 139(2):431–6, 436. [PubMed: 20106404]

13. Hussey GS, Dziki Jenna L.JL, Badylak SF. Extracellular matrix-based materials for regenerative medicine. Nature Reviews Materials, 2018, 3: 159–173.

14. Quint C, Kondo Y, Manson RJ, Lawson JH, Dardik A, Niklason LE. Decellularized tissue-engineered blood vessel as an arterial conduit. Proc Natl Acad Sci U S A, 2011, 108(22):9214–9. [PubMed: 21571635]

15. L'Heureux N, Dusserre N, Konig G, Victor B, Keire P, Wight TN, Chronos NA, Kyles AE, Gregory CR, Hoyt G, Robbins RC, McAllister TN. Human tissue-engineered blood vessels for adult arterial revascularization. Nat Med, 2006, 12(3):361–5. [PubMed: 16491087]

16. Syedain Z, Reimer J, Lahti M, Berry J, Johnson S, Tranquillo RT. Tissue engineering of acellular vascular grafts capable of somatic growth in young lambs. Nat Commun, 2016, 7:12951. [PubMed: 27676438]

17. Dahl SL, Kypson AP, Lawson JH, Blum JL, Strader JT, Li Y, Manson RJ, Tente WE, DiBemardo L, Hensley MT, Carter R, Williams TP, Prichard HL, Dey MS, Begelman KG, Niklason LE. Readily available tissue-engineered vascular grafts. Sci Transl Med, 2011, 3(68):68ra9.

18. Syedain ZH, Graham ML, Dunn TB, O'Brien T, Johnson SL, Schumacher RJ, Tranquillo RT. A completely biological "off-the-shelf" arteriovenous graft that recellularizes in baboons. Sci Transl Med, 2017, 9(414).

19. Lawson JH, Glickman MH, Ilzecki M, Jakimowicz T, Jaroszynski A, Peden EK, Pilgrim AJ, Prichard HL, Guziewicz M, Przywara S, Szmidt J, Turek J, Witkiewicz W, Zapotoczny N, Zubilewicz T, Niklason LE. Bioengineered human acellular vessels for dialysis access in patients with end-stage renal disease: two phase 2 single-arm trials. Lancet, 2016, 387(10032):2026–2034. [PubMed: 27203778]
20. Lupher ML Jr, Gallatin WM. Regulation of fibrosis by the immune system. Adv Immunol. 2006, 89:245–88. [PubMed: 16682276]
21. Hallin RW, Sweetman WR. The Sparks' mandril graft: A seven year follow-up of mandril grafts placed by Charles H. Sparks and his associates. Am J Surg, 1976, 132(2): 221–223. [PubMed: 133619]
22. Sawyer PN, Kaplitt MJ, Sanders RJ, Williams GM, Leather RP, Karmody A, Hallin RW, Taylor R, Fries CC. Ten year experience with the negatively charged glutaraldehyde-tanned vascular graft in peripheral vascular surgery: Initial multicenter trail. Am J Surg, 1987, 154(5):533–537. [PubMed: 3314542]
23. Nakayama Y, Furukoshi M, Terazawa T, Iwai R. Development of long in vivo tissue-engineered "Biotube" vascular grafts. Biomaterials, 2018,185:232–239. [PubMed: 30248647]
24. Sadtler Kaitlyn, Estrellas Kenneth, Allen Brian W., Wolf Matthew T., Fan Hongni, Tam Ada J., Patel Chirag H., Luber Brandon S., Wang Hao, Wagner Kathryn R., Powell Jonathan D., Housseau Franck, Pardoll Drew M., Elisseeff Jennifer H.. Developing a pro-regenerative biomaterial scaffold microenvironment requires T helper 2 cells. Science, 2016, 352(6283): 366–370. [PubMed: 27081073]
25. Campagnolo P, Tsai TN, Hong X, Kirton JP, So PW, Margariti A, Di Bernardini E, Wong MM, Hu Y, Stevens MM, Xu Q. c-Kit^{+} progenitors generate vascular cells for tissue-engineered grafts through modulation of the Wnt/Klf4 pathway. Biomaterials, 2015, 60:53–61. [PubMed: 25985152]
26. Tsiouris A1, Brewer RJ, Borgi J, Nemeh H, Paone G, Morgan JA. Continuous-flow left ventricular assist device implantation as a bridge to transplantation or destination therapy: racial disparities in outcomes. J Heart Lung Transplant. 2013, 32(3):299–304. [PubMed: 23265907]
27. L'Heureux N, McAllister TN, de la Fuente LM. Tissue-engineered blood vessel for adult arterial revascularization. N Engl J Med, 2007, 357(14): 1451–3. [PubMed: 17914054]
28. Sparks CH. Autogenous grafts made to order. Ann Thorac Surg, 1969,8:104–113. [PubMed: 5798828]
29. Nakayama Y, Tsujinaka T. Acceleration of robust "biotube" vascular graft fabrication by in-body tissue architecture technology using a novel eosin Y-releasing mold. J Biomed Mater Res B Appl Biomater, 2014, 102(2):231–8. [PubMed: 23908123]
30. Sparks CH. Silicone mandril method of femoropopliteal artery bypass. Clinical experience and surgical techniques. Am J Surg, 1972, 124:244–249. [PubMed: 5045894]
31. Kott I, Peirce EC, Mitty HA, Geller SA, Jacobson JH. The tissue tube as a vascular prosthesis. Arch Surg, 1973,106:206–207. [PubMed: 4686522]
32. Huynh T, Abraham G, Murray J, Brockbank K, Hagen PO, Sullivan S. Remodeling of an acellular collagen graft into a physiologically responsive neovessel. Nat Biotechnol, 1999 11;17(11): 1083–6. [PubMed: 10545913]
33. Niklason LE. Understanding the Extracellular Matrix to Enhance Stem Cell-Based Tissue Regeneration. Cell Stem Cell, 2018, 22(3):302–305. [PubMed: 29499149]
34. von Bornstädt D, Wang H, Paulsen MJ, Goldstone AB, Eskandari A, Thakore A, Stapleton L, Steele AN, Truong VN, Jaatinen K, Hironaka C, Woo YJ. Rapid Self-Assembly of Bioengineered Cardiovascular Bypass Grafts From Scaffold-Stabilized, Tubular Bilevel Cell Sheets. Circulation, 2018, 138:2130–2144. [PubMed: 30474423]
35. Geelhoed WJ, van der Bogt KEA, Rothuizen TC, Damanik FFR, Hamming JF, Mota CD, van Agen MS, de Boer HC, Restrepo MT, Hinz B, Kislaya A, Poelma C, van Zonneveld AJ, Rabelink TJ, Moroni L, Rotmans JI. A novel method for engineering autologous non-thrombogenic in situ tissue-engineered blood vessels for arteriovenous grafting. Biomaterials, 2020, 229:119577. [PubMed: 31704466]
36. Byrom MJ, Bannon PG, White GH, Ng MK. Animal models for the assessment of novel vascular conduits. J Vasc Surg, 2010, 52(1): 176–195. [PubMed: 20299181]

37. Li L, Terry CM, Shiu YT, Cheung AK. Neointimal hyperplasia associated with synthetic hemodialysis grafts. Kidney Int, 2008, 74(10): 1247–1261. [PubMed: 18668026]
38. Cheung AK1, Terry C, Li L. Pathogenesis and local drug delivery for prevention of vascular access stenosis. J Ren Nutr, 2008, 18(1): 140–145. [PubMed: 18089461]
39. Ott HC, Matthiesen TS, Goh SK, Black LD, Kren SM, Netoff TI, Taylor DA. Perfusion-decellularized matrix: using nature's platform to engineer a bioartificial heart. Nat Med, 2008, 14(2):213–21. [PubMed: 18193059]
40. Olausson M, Patil PB, Kuna VK, Chougule P, Hernandez N, Methe K, Kullberg-Lindh C, Borg H, Ejnell H, Sumitran-Holgersson S. Transplantation of an allogeneic vein bioengineered with autologous stem cells: a proof-of-concept study. Lancet, 2012, 380(9838):230–237. [PubMed: 22704550]
41. Pennel T, Fercana G, Bezuidenhout D, Simionescu A, Chuang TH, Zilla P, Simionescu D. The performance of cross-linked acellular arterial scaffolds as vascular grafts; pre-clinical testing in direct and isolation loop circulatory models. Biomaterials, 2014, 35(24):6311–22. [PubMed: 24816365]
42. Brown BN, Ratner BD, Goodman SB, Amar S, Badylak SF. Macrophage polarization: an opportunity for improved outcomes in biomaterials and regenerative medicine. Biomaterials, 2012, 33(15):3792–802. [PubMed: 22386919]
43. Guillemette MD, Gauvin R, Perron C, Labbé R, Germain L, Auger FA. Tissue-engineered vascular adventitia with vasa vasorum improves graft integration and vascularization through inosculation. Tissue Eng Part A, 2010, 16(8):2617–26. [PubMed: 20455774]
44. Kaushal S,Amiel GE, Guleserian KJ, Shapira OM, Perry T, Sutherland FW, Rabkin E, Moran AM, Schoen FJ, Atala A, Soker S, Bischoff J, Mayer JE Jr. Functional small-diameter neovessels created using endothelial progenitor cells expanded *ex vivo*. Nat Med, 2001, 7(9): 1035–40. [PubMed: 11533707]
45. Karamariti E, Margariti A, Winkler B, Wang X, Hong X, Baban D, Ragoussis J, Huang Y, Han JD, Wong MM, Sag CM, Shah AM, Hu Y, Xu Q. Smooth muscle cells differentiated from reprogrammed embryonic lung fibroblasts through DKK3 signaling are potent for tissue engineering of vascular grafts. Circ Res, 2013, 112(11): 1433–1443. [PubMed: 23529184]
46. Benrashid E, McCoy CC, Youngwirth LM, Kim J, Manson RJ, Otto JC, Lawson JH. Tissue engineered vascular grafts: Origins, development, and current strategies for clinical application. Methods, 2016, 15;99:13–19.
47. Bezhaeva T, Geelhoed WJ, Wang D, Yuan H, van der Veer EP, Alem CMAV, Damanik FFR, Qiu X, Zonneveld AV, Moroni L, Li S, Rotmans JI. Contribution of bone marrow-derived cells to in situ engineered tissue capsules in a rat model of chronic kidney disease. Biomaterials. 2019 2;194:47–56. [PubMed: 30580195]

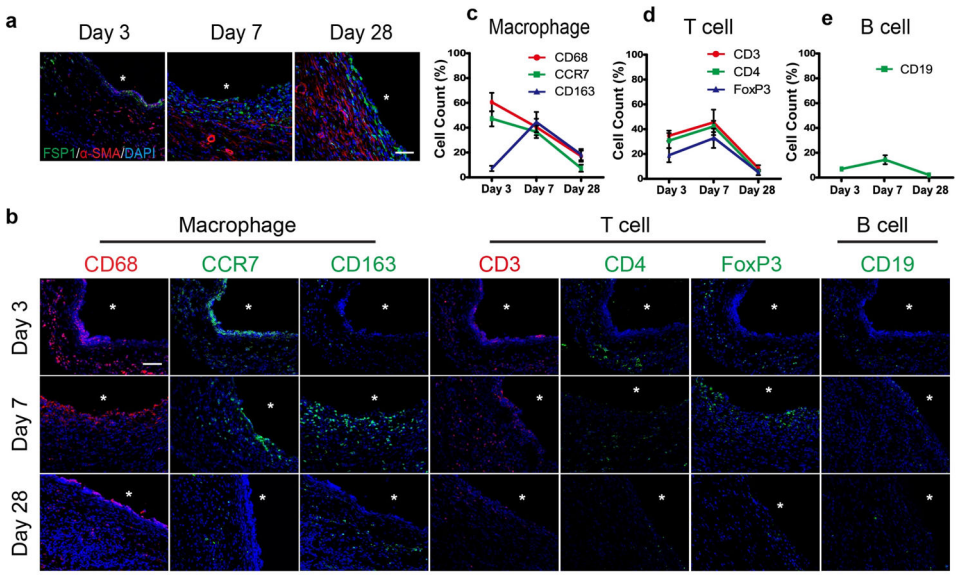

Figure 1.

Immune responses during fibrotic capsule formation around a subcutaneously implanted Teflon mandrel. To make fibrotic conduits, Teflon mandrels were implanted into the subcutaneous pouches in the abdominal wall of rats. The cross sections of fibrotic tissues at days 3, 7 and 28 were analyzed by immunostaining and fluorescence microscopy, **(a)** Immunostaining for fibroblast markers FSP1 (green) and α-SMA (red). Nuclei were stained by DAPI (blue), **(b)** Immunostaining for CD68 (Pan-macrophage), CCR7 (M1 macrophage r), CD163 (M2 macrophage), CD3 (T lymphocyte), CD4 (Helper T-cell subset), FoxP3 (Regulatory T-cell) and CD19 (B lymphocyte), **(c)** Percentage of CD68, CCR7 and CD163 positive cells. **(d)** Percentage of CD3, CD4 and FoxP3 positive cells, **(e)** Percentage of CD19 positive cells. Scale bars: 50 μm. Lumen is marked with *. (n=6)

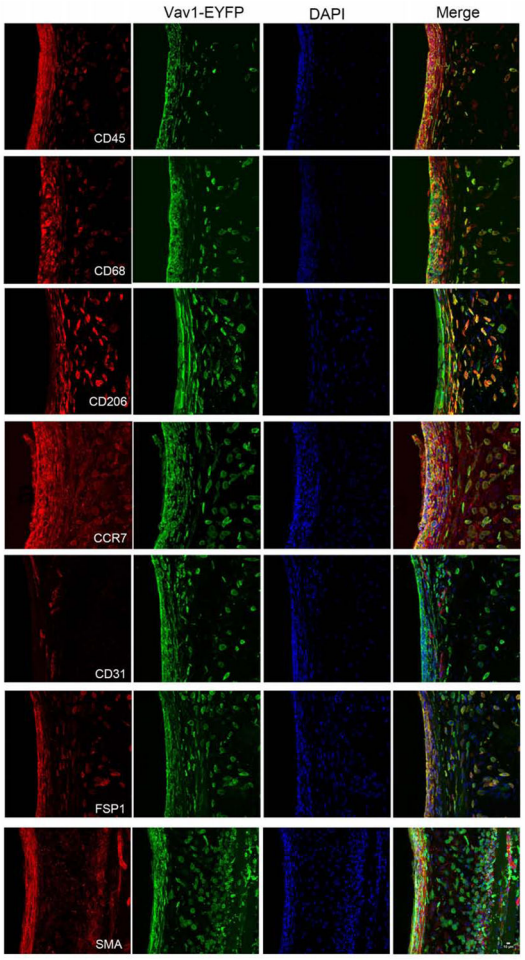

Figure 2.

Lineage tracing of inflammatory cell-derived cells in fibrotic capsule in transgenic mice. Teflon mandrels were implanted subcutaneously in Vav1-cre/R26R-EYFP mice for 7 days. The cross sections of fibrotic tissues were analyzed by immunostaining for CD45, CD68, CCR7, CD206 (M2 macrophage), CD31, FSP1 or α-SMA (in red). Hematopoietic cell-derived cells were labeled by EYFP Cell nuclei were stained with DAPI. Scale bar: 50 μm. (n=3)

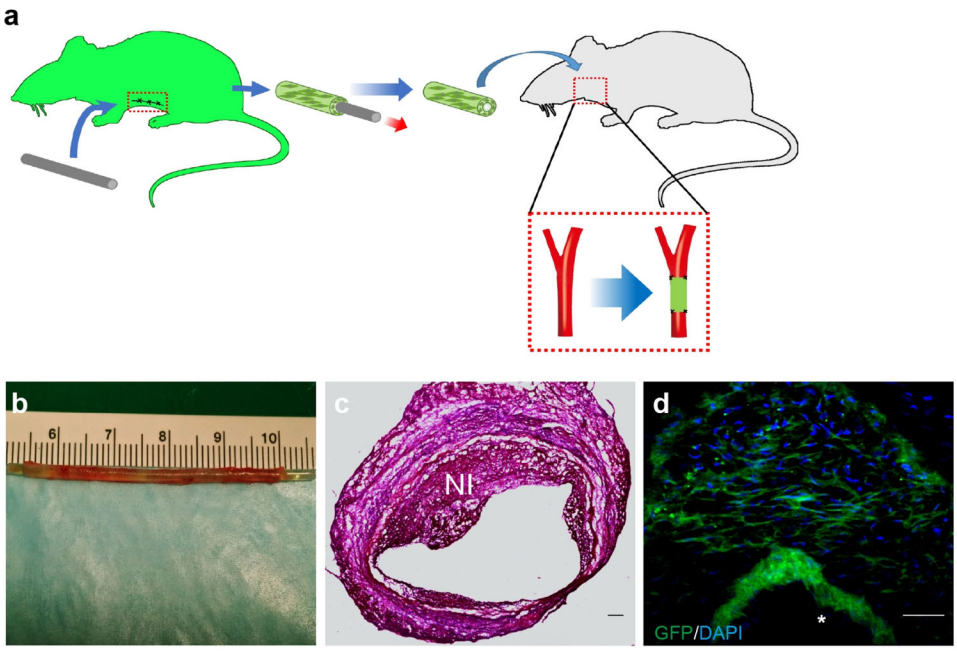

Figure 3.

Contribution of cells in fibrotic conduits to neointima formation after implantation as a vascular graft, **(a)** Fibrotic conduits were made by subcutaneous implanting Teflon mandrels into GFP Sprague-Dawley rat for 4 weeks. The fibrotic conduits were implanted into the carotid artery of Sprague-Dawley rats as vascular grafts with the administration of Cyclosporin A (CyA, 6 mg/kg). **(b)** The vascular grafts were explanted after 4 weeks. **(c)** Hematoxylin and eosin (H&E) staining of explanted a vascular graft. **(d)** Distribution of GFP^+ cells in the neointima (labeled by NI). Scale bar: 50 μm. Lumen is marked with *. (n=6)

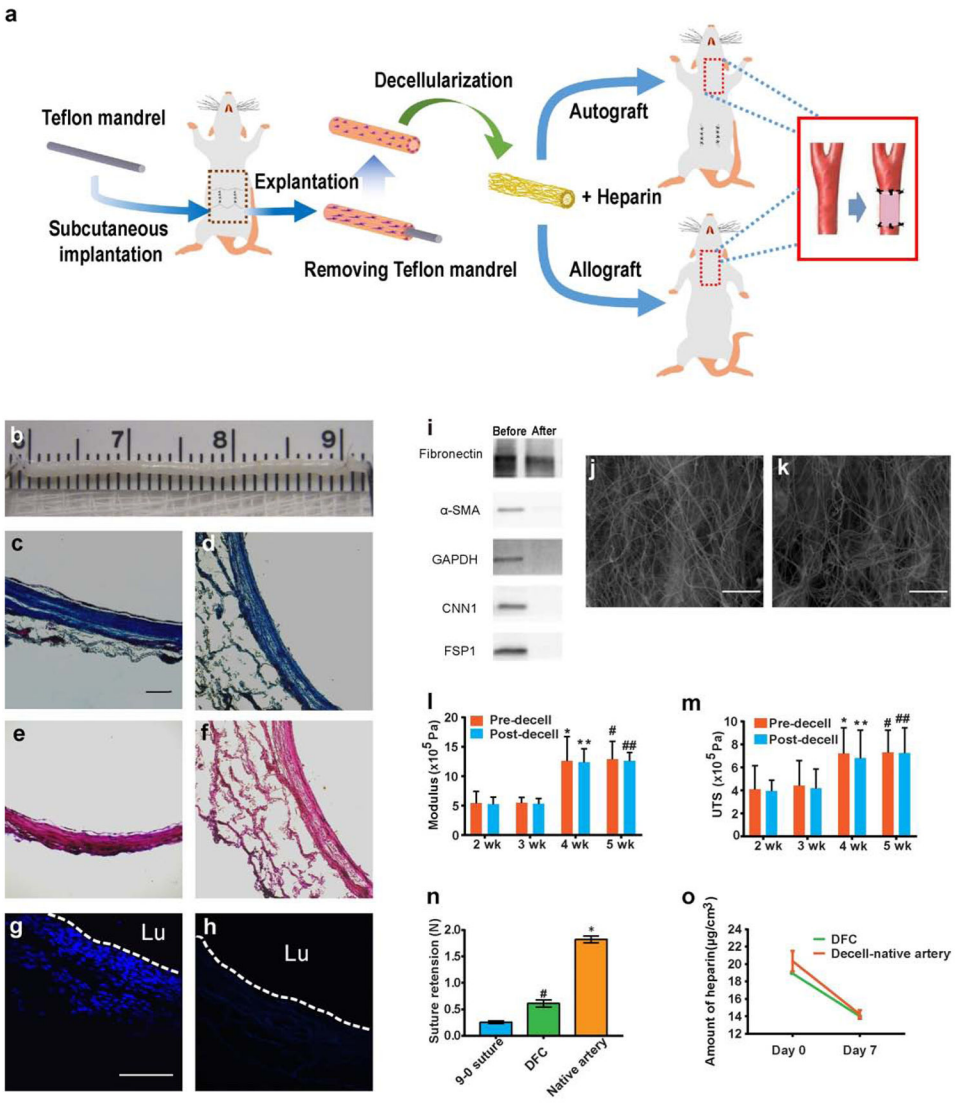

Figure 4.

Fabrication and characterization of DFCs. **(a)** Schematic showing the fabrication, modification and implantation of DFCs. **(b)** The gross appearance of a DFC before implantation. **(c-d)** Histological analysis of the cross sections of DFCs by Masson's trichrome staining before (c) and after (d) decellularization, demonstrating the preservation of collagen(blue). **(e-f)** Verhoeff's staining before (e) and after (f) decellularization, showing no elastin in the matrix. **(g-h)** DAPI staining of cross sections showing cells before (g) and after decellularization (h). Scale bars: 100 μm in c-h. **(i)** Western blotting analysis of major cellular proteins to further confirm that all cellular components were removed. **(j-k)** SEM images of the inner (j) and outer (k) surface of a DFC. Scale bars: 50 μm. **(l-m)** Comparison of mechanical properties of fibrotic conduits, including Young's modulus (l) and ultimate tensile strength (UTS) (m), before and after decellularization at 2, 3, 4 and 5 weeks. (n=9) **(n)** Suture retention of DFCs at 4 weeks and native arteries. (n=6) #P < 0.05, DFC versus 9-0 suture. *P < 0.05, native artery versus DFC. **(o)** The amount of heparin conjugated on

DFC and the decellularized native artery at day 0 and day 7 under flow conditions *in vitro.* Data represent mean ± S.D.

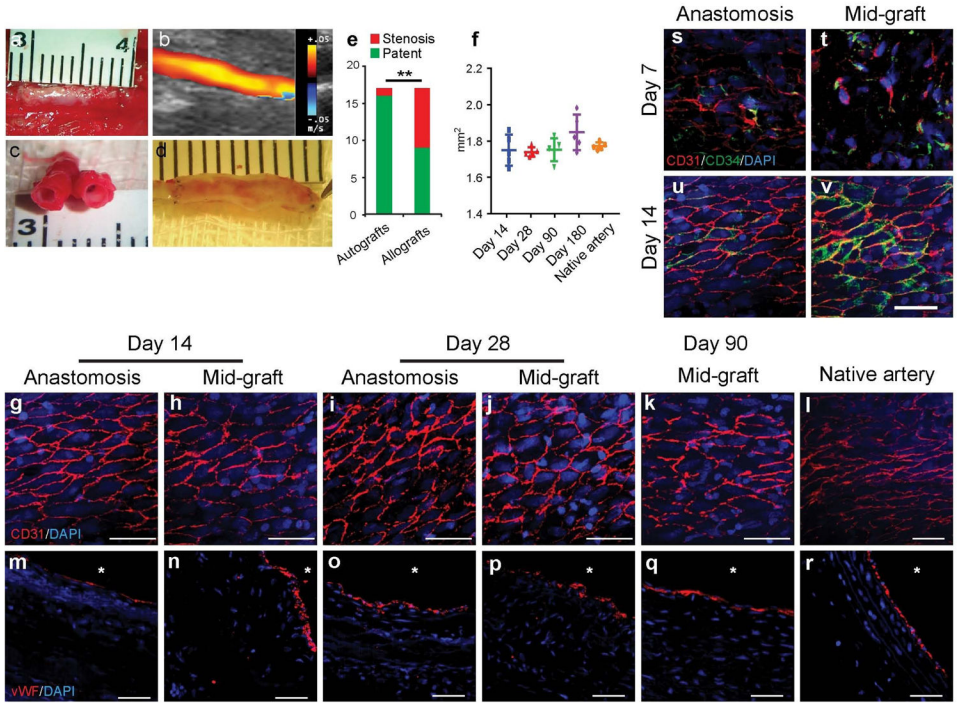

Figure 5.

Patency and endothelialization of the grafts at days 14, 28 and 90. **(a-d)** Patent grafts at day 90 after implantation, showing the gross appearance of a neoartery (a), the ultrasound imaging of a graft (b), the cross-sectional structure (c), and longitudinal-sectional structure (d). **(e)** Comparison of the patency rates of the autografts and the allografts at day 90 after implantation. **(f)** Luminal area of remodeling grafts at different time points and native common carotid arteries. Data represent mean ± S.D. **(g-r)** Analysis of endothelialization by immunostaining for EC markers in the grafts. *En face* immunostaining for CD31 (red) (g-k) and cross-sectional immunostaining for vWF (red) (m-q) of the explanted grafts at days 14, 28 and 90 after implantation. Nuclei were stained by DAPI (blue). The staining of native common carotid artery was as a positive control (l, r). Scale bars: 50 μm. Lumen is marked with *. **(s-v)** EPCs contributed to endothelialization of DFCs. *En-face* staining of the anastomotic site and mid-graft for CD34 (green) and CD31 (red) (red) at days 7 and 14 after re-implantation. Scale bar: 50 μm.

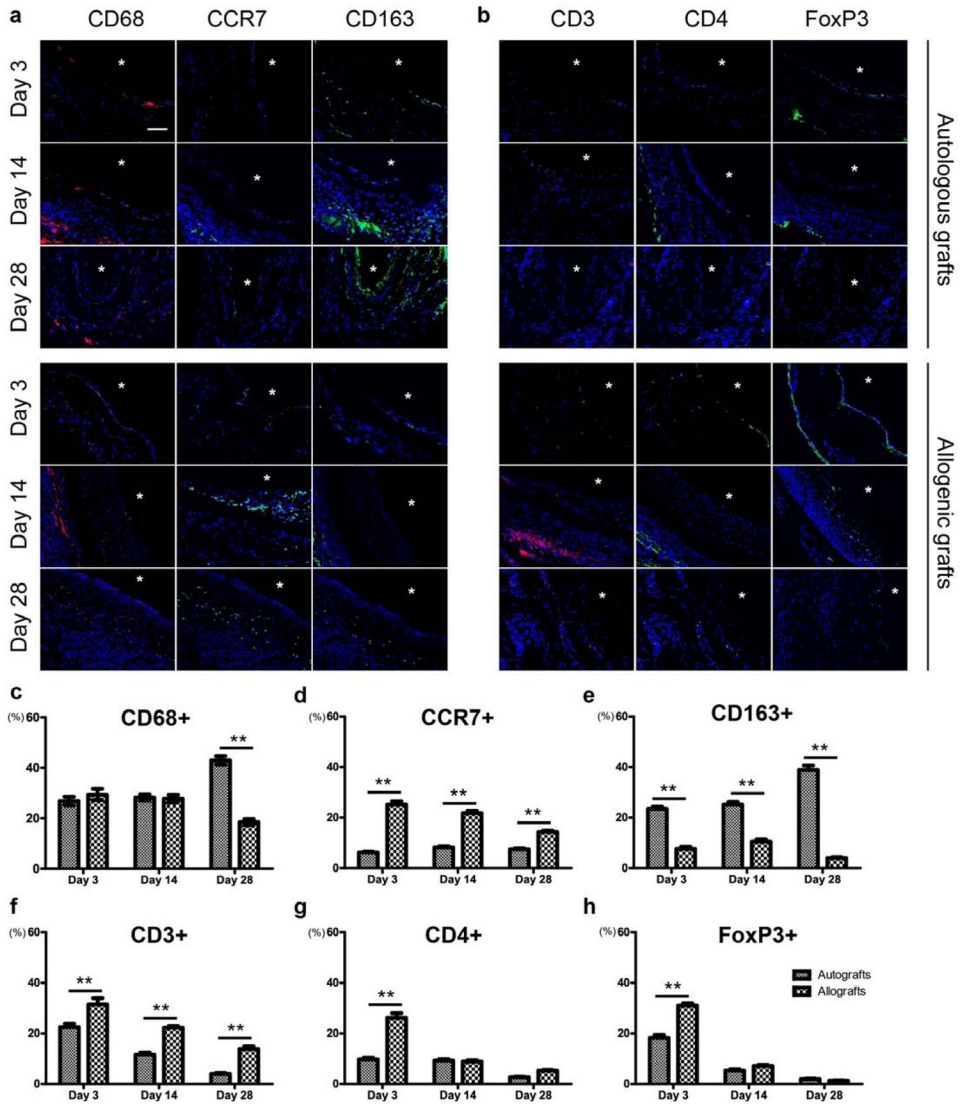

Figure 6.

Comparison of the inflammatory responses in autografts and allografts. **(a)** Immunostaining of cross-sections for macrophage markers at days 3, 14 and 28. **(b)** Immunostaining of cross-sections for T cell markers at days 3, 14 and 28. Lumen is marked with *. Scale bars: 50 μm. **(c-h)** Percentage of macrophages **(c, d, e)** and T lymphocytes **(f, g, h)** in the autografts and the allografts (* $P < 0.05$, ** $P < 0.01$). Data represent mean ± S.D. At least 15 fields of the same graft were pooled for cell counting. (n=5)

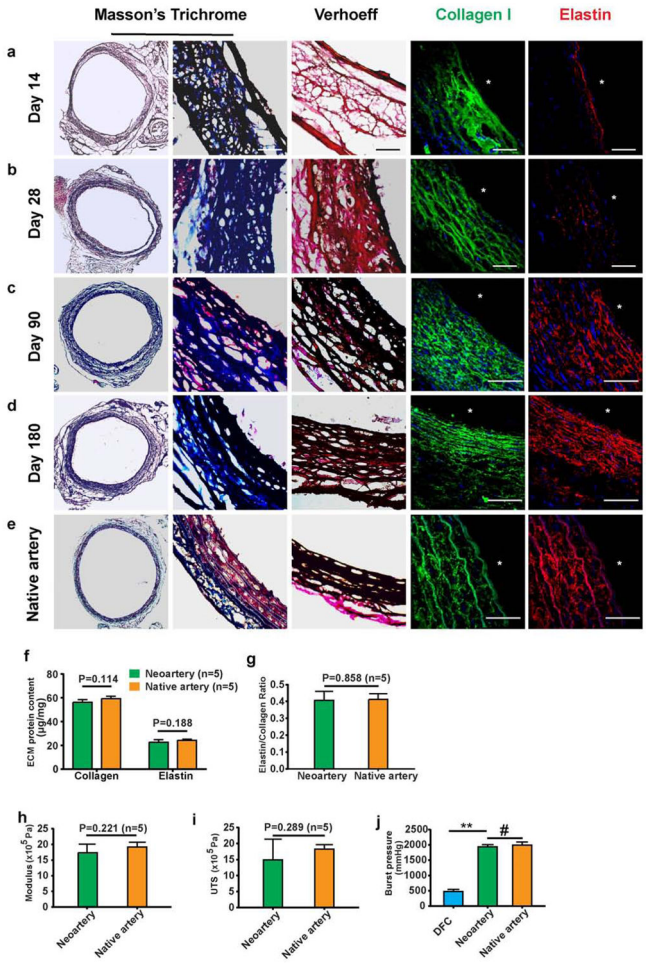

Figure 7.

ECM remodeling of autografts. **(a-d)** The structure and contents of collagen and elastin at days 14 (a), 28 (b), 90 (c) and 180 (d) after implantation were examined by histological staining of cross sections. Collagen (blue) and elastin (black) were detected by Masson's trichrome and Verhoeff's staining respectively. Specific immunostaining for collagen I (green) and elastin (red) was also performed. Nuclei were stained by DAPI (blue). **(e)** The staining of native common carotid artery was used as a positive control. Scale bars: 50 μm (a-e). Lumen is marked with *. **(f-h)** Comparison of mechanical properties of the neoartery at 90 days with the native common carotid artery, including Young's modulus (f), ultimate tensile strength (g) and burst pressure (** $P < 0.01$, # $P > 0.05$) (h). **(i, j)** ECM contents of the neoartery at day 90 and native common carotid artery were quantified. Data represent mean ± S.D. (n=5)

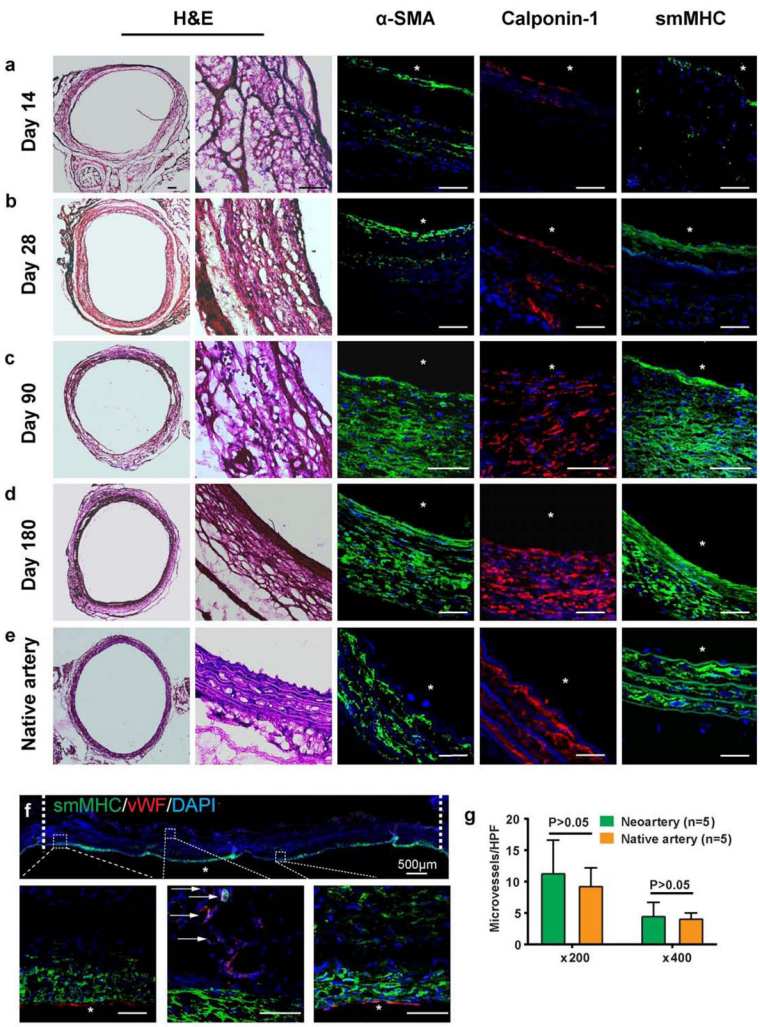

Figure 8.

Re-cellularization in the wall of autografts. **(a-e)** Cell recruitment and SMC differentiation at days 14 (a), 28 (b), 90 (c) and 180 (d) after implantation. The columns showed H&E staining and immunostaining for α-SMA (green), Calponin-1 (red) and smMHC (green). Nuclei were stained by DAPI (blue). The native common carotid artery was used as a positive control (e). Scale bars: 50 μm. **(f)** Longitudinal examination of autografts at days 90 after implantation. The graft was split and cryosectioned longitudinally and stained for vWF and smMHC. Lower left: magnified view of the anastomotic site; lower right: magnified view of the mid-graft; middle: Arrows indicate *vasa vasorum* around the outer wall; the dashed lines indicate the anastomotic sites. Scale bars in the lower panels: 50 μm. **(g)** The density of the microvessels around the graft at 90 days and that around the native common carotid artery are compared ($P > 0.05$). Data represent mean ± S.D. Lumen is marked with *. HPS: high power field. (n=5)